

Atmospheric Pressure Loading

Dudy D. Wijaya, Johannes Böhm, Maria Karbon, Hana Krásná and Harald Schuh

Abstract Loading of the Earth's crust due to variations of global atmosphere pressure can displace the positions of geodetic sites by more than 1 cm both vertically and horizontally on annual to sub-diurnal time scales, and thus has to be taken into account in the analysis of space geodetic observations. This part of the book discusses methods for the calculation of the displacements. In particular, it summarizes the simple approach with regression coefficients between surface pressure and the vertical displacement and the more rigorous geophysical approach with load Love numbers and Green's functions. Furthermore, we describe the special treatment of the thermal tides (S1 and S2), the importance of the reference pressure, as well as the inverted barometer hypothesis for the oceans. Finally, we present space geodetic results with the application of those correction models for the analysis of Very Long Baseline Interferometry observations.

D. D. Wijaya (✉)
Geodesy Research Group, Institute of Technology Bandung,
Ganesha 10, Bandung-West Java, Indonesia
e-mail: dudy@gd.itb.ac.id

J. Böhm · H. Krásná
Department of Geodesy and Geoinformation, Vienna University of Technology,
Gußhausstraße 27-29, 1040 Vienna, Austria
e-mail: johannes.boehm@tuwien.ac.at

H. Krásná
e-mail: hana.krasna@tuwien.ac.at

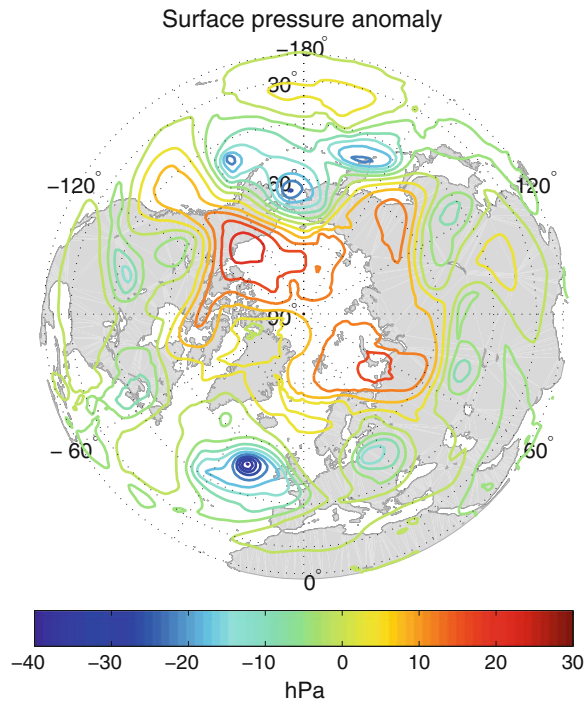
M. Karbon
Section 1.1 GPS/Galileo Earth Observations, Helmholtz Centre Potsdam GFZ German Research
Centre for Geosciences, Telegrafenberg A 17, 14473 Potsdam, Germany
e-mail: karbon@gfz-potsdam.de

H. Schuh
Department 1 Geodesy and Remote Sensing, Helmholtz Centre Potsdam GFZ German Research
Centre for Geosciences, Telegrafenberg A 17, 14473 Potsdam, Germany
e-mail: schuh@gfz-potsdam.de

1 Surface Pressure Variations and Deformation of the Solid Earth

Differential heating between low and high latitudes gives rise to atmospheric motions on a wide range of scales. Prominent features of the so-called atmospheric general circulation include westerly (west-to-east) mid-latitude tropospheric jet streams and lower mesospheric jet streams. Superimposed on the jet streams are eastward propagating baroclinic waves that are one of a number of types of weather systems. Examples of baroclinic waves are cyclones and anticyclones, which are representing variations of low and high air pressure from mean pressure (Wallace and Hobbs 2006). Figure 1 shows spatial variations of surface pressure anomaly (the pressure minus a mean of the pressure field) over the Northern hemisphere (10–90°N) at 00 UTC on January 1, 2010. The highest pressure anomaly (≈ 25 hPa) is over the far northern portions of Siberia and North America extending into the Arctic Ocean. The lowest pressure anomaly (≈ -35 hPa) is over the middle Atlantic Ocean, south of Iceland. Both cyclones and anti-cyclones typically have spatial extent between some hundreds (tropical cyclones) and some thousands (continental anti-cyclones) of kilometers. Their duration is generally of the order of a few days and sometimes they can remain stable for weeks (Rabbel and Zschau 1985).

Fig. 1 Surface pressure anomaly (the pressure minus a mean of the pressure field) over Northern hemisphere (10–90°N) from data of the European Centre for Medium-range Weather Forecast (ECMWF) at 00 UTC on January 1, 2010



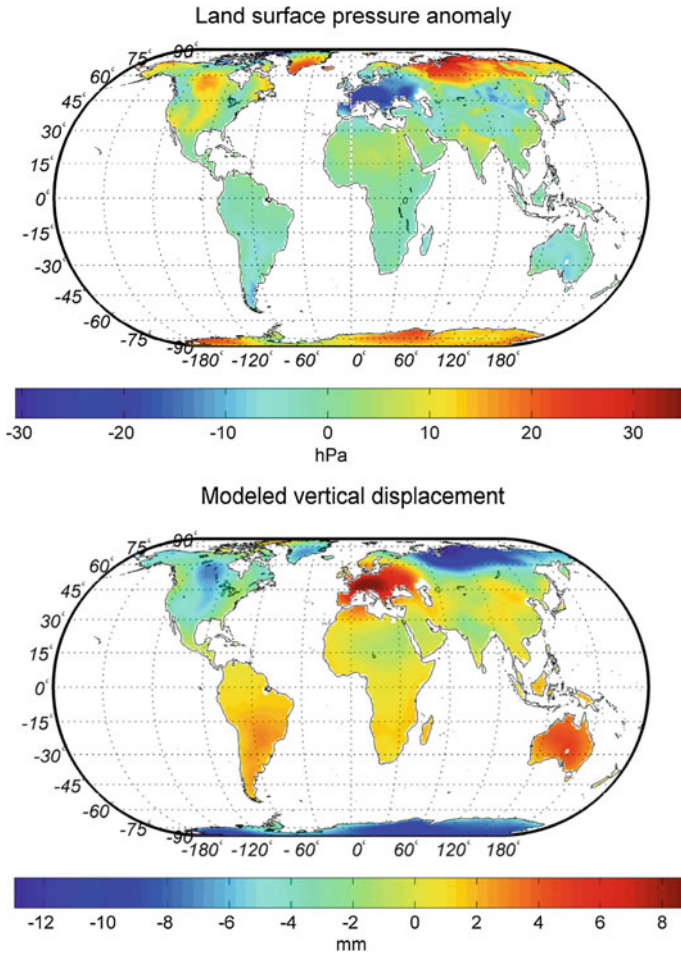


Fig. 2 Spatial variations of surface pressure anomaly and modeled vertical displacements at 00 UTC on January 1, 2010

Complex interactions between the Earth and the atmosphere lead these global atmospheric pressure variations to produce several geodynamic effects as e.g. surface load deformations (Farrell 1972; Rabbel and Zschau 1985; van Dam and Wahr 1987), changes of the gravity potential (Farrell 1972; Boy and Chao 2009), and variations in the Earth’s rotational motion (Wahr 1983). In the context of surface load deformations, global variations in surface pressure can displace the Earth’s surface by more than 1 cm both vertically and horizontally on annual to sub-diurnal timescales. Figure 2 shows spatial variations of land surface pressure and modeled vertical displacements over the globe with an obvious negative correlation. A large (positive) pressure anomaly of about 30 hPa over Siberia deforms the Earth’s surface by about 10 mm. On the other side, a negative pressure anomaly (≈ -20 hPa) over Europe uplifts the region. The magnitude of atmospheric pressure loading (APL) effects for

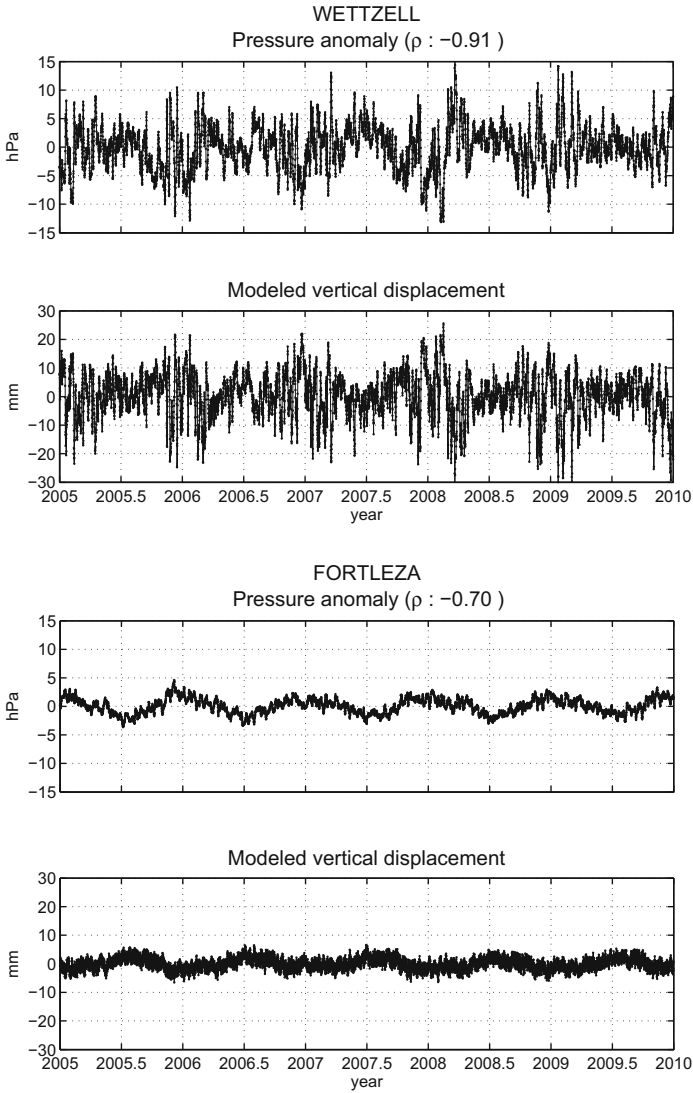


Fig. 3 Temporal variation of pressure anomalies and modeled vertical displacements at stations Wetzell (Germany) and Fortaleza (Brazil) from 2005.0 to 2010.0

a particular area depends primarily on geographical latitude and proximity to the oceans where the inverted barometer (IB) effects are significant. It can be seen that variations of pressure anomaly at mid-latitudes are large and, therefore, the effects of APL in this region are more dominant than those in other regions.

Figure 3 shows temporal variations of pressure anomalies and the corresponding vertical displacements for the two geodetic stations Wetzell, Germany (49.15°N) and Fortaleza, Brazil (3.88°S) with correlation coefficients between -0.9 and -0.7 .

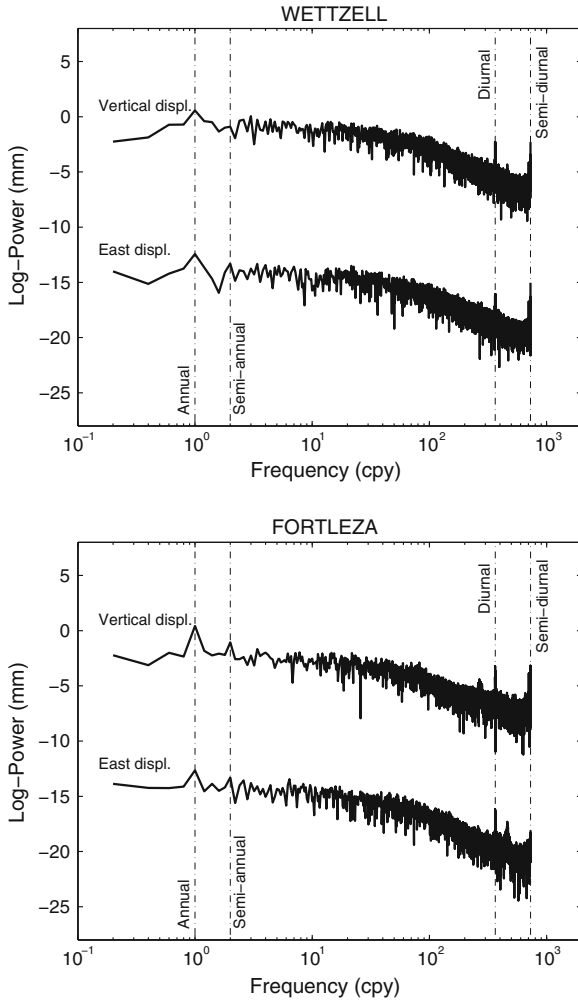


Fig. 4 Amplitude spectra of the displacements in vertical and east directions at stations Wetzell (Germany) and Fortaleza (Brazil). The amplitude of the east direction is translated by $\log(10^5)$

The displacements at Fortaleza are typical for coastal and lower latitude sites. The magnitude of the variations is fairly low due to smaller pressure fluctuation near the equator. Because of the IB effects, the magnitude of APL effects is also further reduced by the site’s proximity to the Atlantic Ocean. The displacements at a mid-latitude and non-coastal site (Wetzell) indicate large vertical variations with amplitudes in the order of 5–15 mm. The horizontal displacements are subjected to similar temporal variations with magnitudes of approximately three times smaller than those of the vertical displacements (not shown here).

The amplitude spectra of the displacements in vertical and east directions (Fig. 4) shows significant narrow-band diurnal and semi-diurnal signals. Petrov and Boy (2004) mentioned that strong wide-band annual and semi-annual signals and relatively weak signal for period below 10 days, except strong peaks at the diurnal and semi-diurnal bands, are typical for the displacements at low-latitude stations. In the mid-latitude regions, peak-to-peak variations in the vertical direction occur with a period of about 5–12 days that correspond to the circulations of high and low pressure structures in this regions, partly due to baroclinic variability (Dell’Aquila et al. 2005). These timescales represent the limit of validity of the IB assumption for describing the oceanic response to atmospheric pressure forcing.

The effects of APL have been observed in high-precision space geodetic data, i.e., Very Long Baseline Interferometry (VLBI) (van Dam and Wahr 1987; MacMillan and Gipson 1994; Petrov and Boy 2004; Böhm et al. 2007), Global Navigation Satellite Systems (GNSS) (van Dam and Herring 1994; van Dam et al. 1994; Tregoning and van Dam 2005; Dach et al. 2011), and Satellite Laser Ranging (SLR) (Bock et al. 2005). These observational data are often used for geodynamic studies and can be important to remove the displacement signals due to APL, which otherwise propagate into other parameters and effects like hydrological loading and tropospheric delay estimation. For the purpose of correcting APL signals in space geodetic observations, it is necessary to provide the model and corrections for routine data reduction. In the following sections, different approaches to model APL corrections will be discussed.

2 Modeling Atmosphere Pressure Loading

The IERS (International Earth Rotation and Reference Systems Service) Conventions 2010 (Petit and Luzum 2010) describe two possibilities to model the APL effects: (i) a geophysical approach using convolution of the actual loading distribution over the entire surface of the solid Earth, (ii) an empirical model which is based on the actual deformations derived from geodetic observations taken at individual sites. Both approaches will be described in this section.

2.1 Geophysical Approach

Farrell (1972) considered the elastic yield of the solid Earth to changing surface loads and solved the point loading problem for a spherically symmetric, non-rotating, elastic, and self-gravitating Earth with a liquid core, by devising the Green’s functions, which encompass the Earth’s response, over spherical harmonic degrees. The essential step in the calculation of surface displacements due to loading comprises the global convolution of the load influence, which is represented by the corresponding Load Love Numbers (LLN) inside the Green’s functions, see Eqs. (4) and (5).

As for the mathematical formulation, let \mathbf{r} be the position of an arbitrary station where the surface deformation shall be determined. The station displacements (vertical, east and north directions) evoked by surface pressure loads $P(\mathbf{r}', t)$ over the entire surface of the Earth S are written as:

$$U_r(\mathbf{r}, t) = \iint_S [P(\mathbf{r}', t) - P_{ref}(\mathbf{r}')] G_r(\psi) \cos \vartheta' d\vartheta' d\lambda', \quad (1)$$

$$U_e(\mathbf{r}, t) = \iint_S [P(\mathbf{r}', t) - P_{ref}(\mathbf{r}')] G_h(\psi) \sin \alpha_{\mathbf{r}\mathbf{r}'} \cos \vartheta' d\vartheta' d\lambda', \quad (2)$$

$$U_n(\mathbf{r}, t) = \iint_S [P(\mathbf{r}', t) - P_{ref}(\mathbf{r}')] G_h(\psi) \cos \alpha_{\mathbf{r}\mathbf{r}'} \cos \vartheta' d\vartheta' d\lambda'. \quad (3)$$

$P_{ref}(\mathbf{r}')$ denotes the reference pressure, which represents the pressure of an unperturbed atmosphere. Various methods for determination of the reference pressure are summarized by Schuh et al. (2009). ϑ' is the geocentric latitude and λ' is the longitude. The Green's functions are computed from Load Love Numbers (LLNs) h'_n and l'_n according to

$$G_r(\psi) = \frac{GR}{g^2} \sum_{n=0}^{\infty} h'_n P_n(\cos \psi), \quad (4)$$

$$G_h(\psi) = \frac{GR}{g^2} \sum_{n=0}^{\infty} l'_n \frac{\partial P_n(\cos \psi)}{\partial \psi}, \quad (5)$$

where G is the universal gravitational constant, ψ is the angular distance between the station with the position \mathbf{r} and the pressure source with the position \mathbf{r}' g is the mean gravitational acceleration at the surface of the Earth, R is the mean Earth radius and P_n is the Legendre polynomial of degree n .

Cosine and sine of the azimuth angle $\alpha_{\mathbf{r}\mathbf{r}'}$ between the station and the pressure load can be calculated using the formalism described by Hofmann-Wellenhof and Moritz (2005):

$$\cos \alpha_{\mathbf{r}\mathbf{r}'} = \frac{\cos \vartheta \sin \vartheta' - \sin \vartheta \cos \vartheta' \cos(\lambda' - \lambda)}{\sin \psi} \quad (6)$$

$$\sin \alpha_{\mathbf{r}\mathbf{r}'} = \frac{\cos \vartheta' \sin(\lambda' - \lambda)}{\sin \psi} \quad (7)$$

In the calculation, a complex IB model describing the oceanic response to atmospheric pressure and wind forcing should be introduced (Geng et al. 2012). Instead of using such a complex model, van Dam and Wahr (1987) proposed a

slightly modified IB hypothesis. If there is a net increase or decrease in the mass of air above the oceans, the seafloor experiences a uniform pressure $\Delta\bar{P}_o$ acting everywhere on the ocean bottom surface:

$$\Delta\bar{P}_o = \frac{\iint_{ocean} [P(\mathbf{r}', t) - P_{ref}(\mathbf{r}')] \cos \vartheta' d\vartheta' d\lambda'}{\iint_{ocean} \cos \vartheta' d\vartheta' d\lambda'}. \quad (8)$$

The IB model above is adequate to describe the sea height variations with periods longer than 5–20 days but is not accurate enough for shorter periods. Wunsch and Stammer (2010) showed that the (non-equilibrium) diurnal and sub-diurnal ocean tides imply that the global oceanic response is certainly not an IB at shorter periods.

Following Petrov and Boy (2004), the integrals in Eqs. (1), (2) and (3), can be split up into land and ocean contributions, thus an IB correction for the oceanic portion can be applied:

$$U_r(\mathbf{r}, t) = \iint_{land} [P(\mathbf{r}', t) - P_{ref}(\mathbf{r}')] G_r(\psi) ds + \Delta\bar{P}_o \iint_{ocean} G_r(\psi) ds, \quad (9)$$

$$U_e(\mathbf{r}, t) = \iint_{land} [P(\mathbf{r}', t) - P_{ref}(\mathbf{r}')] G_h(\psi) \sin \alpha_{\mathbf{r}\mathbf{r}'} ds + \Delta\bar{P}_o \iint_{ocean} G_h(\psi) \sin \alpha_{\mathbf{r}\mathbf{r}'} ds, \quad (10)$$

$$U_n(\mathbf{r}, t) = \iint_{land} [P(\mathbf{r}', t) - P_{ref}(\mathbf{r}')] G_h(\psi) \cos \alpha_{\mathbf{r}\mathbf{r}'} ds + \Delta\bar{P}_o \iint_{ocean} G_h(\psi) \cos \alpha_{\mathbf{r}\mathbf{r}'} ds, \quad (11)$$

where $ds = \cos \vartheta' d\vartheta' d\lambda'$.

In order to calculate the displacements using Eqs. (9)–(11), the following physical information is required:

- **Global surface pressure.** The parameter $P(\mathbf{r}', t)$ can be derived from data from a Numerical Weather Model (NWM), e.g. from those of the European Centre for Medium-range Weather Forecasts (ECMWF) and the National Centers for Environmental Prediction (NCEP). Both centers provide the data every 3 or 6 h with various spatial resolutions.
- **Reference pressure.** $P_{ref}(\mathbf{r}')$ can be determined by long-term averaging of surface pressure data. Schuh et al. (2009) thoroughly review various methods for the definition of reference pressure for geodetic applications and they propose a new method that is called the Global Reference Pressure (GRP) which is based on the application of pressure level data instead.
- **Green's functions and Load Love Numbers.** The vertical and horizontal Green's functions ($G_r(\psi)$ and $G_h(\psi)$) are used as weighting factors for surface pressure anomaly data $[P(\mathbf{r}', t) - P_{ref}(\mathbf{r}')]$. In the definition of the Green's functions, high

degree LLN are required. Farrell (1972) suggest to compute the LLN values up to degree $n = 10000$.

- **Land-sea mask.** For separation of the integration over land and the oceans, appropriate land-sea masks should be provided. Topography models can be used to generate land-sea masks with various spatial resolutions.

Surface pressure data of the ECMWF or NCEP are known to contain signals associated with the diurnal $S_1(p)$ and semi-diurnal $S_2(p)$ atmospheric tides. Unfortunately, the representation of these tides is significantly distorted owing to the sampling interval of 6 hours of most numerical weather models. This particularly holds for the $S_2(p)$ tide (van den Dool et al. 1997; Petrov and Boy 2004), which is located exactly at the Nyquist frequency of 2 cycles/day and, thus, cannot be modeled correctly. Ponte and Ray (2002) suggested to remove the diurnal and semi-diurnal tidal power from the six-hourly atmospheric pressure fields and re-calculate them using a harmonic model. This leads to the calculation of the displacement corrections in three steps:

1. Calculate non-tidal loading displacements using pressure fields in which the tidal signals have been removed (Sect. 2.1.1).
2. Calculate tidal loading displacements using a gridded global model of pressure tides (Sect. 2.1.2).
3. Calculate total loading displacements by summing both non-tidal and tidal loading displacements.

2.1.1 Non-Tidal Loading Displacements

Petrov and Boy (2004) removed the diurnal and semi-diurnal tidal power from the six-hourly atmospheric pressure fields by subtracting gridpoint-wise sinusoids with the frequencies 1 and 2 cycles/day, that were estimated from several years of six-hourly surface pressure data. As amplitude and phase of sub-daily tidal variations are only quasi-harmonic quantities and might change considerably over time, this approach cannot account for the full $S_1(p)$ and $S_2(p)$ pressure variations. Moreover, it also neglects the seasonal modulation of atmospheric tides, which is manifested in spectral domain as small side lobes around the main frequencies of 1 and 2 cycles/day. However, it has been shown that such an approach is appropriate for correcting APL effects at globally distributed VLBI sites (Petrov and Boy 2004). Most importantly, it is well suited for the operational calculations because it can also be used for real-time applications. An alternative method has been applied by Tregoning and van Dam (2005), who convolved the plain pressure data and then employed a low-pass filter on the time series of the displacements. Note that both approaches only aim at removing the $S_1(p)$ and $S_2(p)$ tidal signals as they are contained in the six-hourly data, regardless of whether their representation in the undersampled meteorological data is accurate or not. Another possibility is the determination of a sinusoidal model from three-hourly numerical weather model data which is then removed from the surface pressure data.

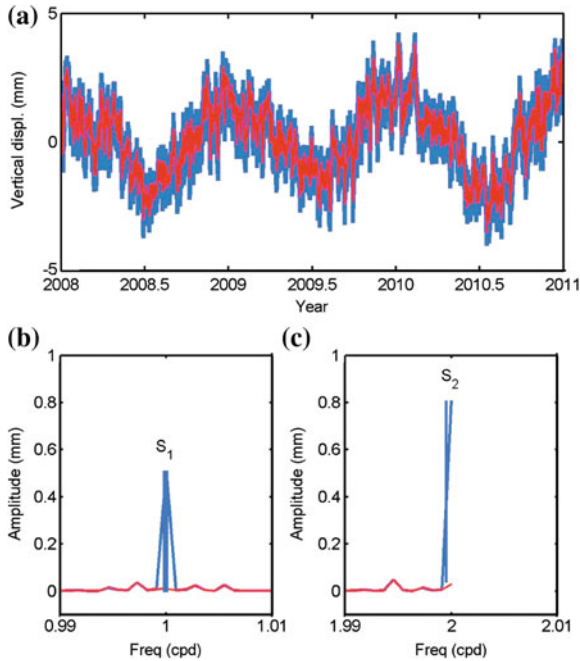


Fig. 5 a Time series with (*blue*) and without (*red*) tidal loading of vertical displacements at Fortaleza, Brazil and (b,c) the corresponding amplitude spectra of atmospheric loading signals

Following Petrov and Boy (2004), we derived the pressure tide model for each node of a 1° global grid of the ECMWF by estimating mean pressure, sine and cosine amplitudes of the $S_1(p)$ signal, and sine and cosine amplitudes of the $S_2(p)$ signal in the six-hourly pressure level data over the period from 1980.0 to 2011.0. After subtracting the modeled sinusoids from six-hourly pressure fields, Eqs. (9)–(11) were applied in order to obtain non-tidal loading displacements. Figure 5 shows the non-tidal loading vertical displacements at Fortaleza station (low-latitude, 3.88°S) in the time domain and the amplitude spectra of the corresponding atmospheric loading signals. Strong peaks containing tides at the frequencies of $S_1(p)$ and $S_2(p)$ are reduced to negligible magnitudes when the tidal signals in surface pressure are removed. The total loading displacement is the sum of non-tidal displacement and the harmonic model of tidal loading displacements (see Sect. 2.1.2).

Examples for signals of non-tidal loading displacements at Fortaleza and Wettzell (mid-latitude, 49.15°N) in vertical and horizontal directions are shown in Fig. 6. The horizontal displacements are derived by taking the square-root of the sum of the squares of the East and North components. The displacements at Fortaleza are typical for coastal and lower latitude sites as the variations are fairly low due to smaller pressure fluctuations near the equator and because of the IB effect, due to the proximity to the Atlantic Ocean. The displacements at a mid-latitude and non-coastal site (Wettzell) indicate large vertical variations in the order of 5–15 mm.

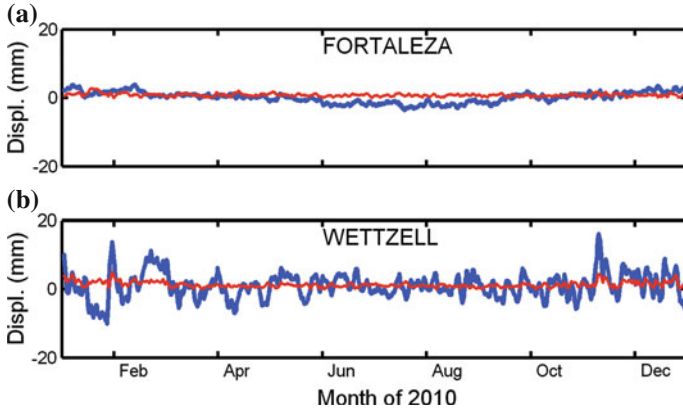


Fig. 6 Non-tidal loading displacements at Fortaleza, Brazil and Wetzell, Germany in vertical (blue) and horizontal (red) directions. The horizontal displacements are derived by taking the square-root of the sum of the squares of the East and North components

Examining Fig. 6b, we find that peak-to-peak variations in the vertical direction occur with a period of about 5–12 days which corresponds to the circulations of high and low pressure structures in mid-latitude regions, partly due to baroclinic variability (Dell’Aquila et al. 2005). These timescales also represent the limit of validity of the IB assumption for describing the oceanic response to atmospheric pressure forcing. It is obvious that the displacements contain annual (Fig. 5a) as well as sub-seasonal signals (Fig. 6b), with increasing magnitude during the winter months.

2.1.2 Tidal Loading Displacements

To account for tidal loading displacements, Ponte and Ray (2002) developed a gridded global model of $S_1(p)$ and $S_2(p)$ pressure tides using the six-hourly field of the ECMWF operational analysis. The $S_2(p)$ standing wave was propagated by applying the interpolation procedure proposed by van den Dool et al. (1997). Comparisons with “ground station” tidal estimates at meteorological stations suggest that their model is reasonably realistic and, thus, it has been recommended in the IERS Conventions 2010 (Petit and Luzum 2010). However, a large drawback remains, as the resulting spatial variations of amplitude and phase of atmospheric tides are somewhat too smooth, especially for the $S_2(p)$ tide (Petrov and Boy 2004). This disadvantage is due to the interpolation procedure that requires filtering out non-migrating tidal components.

At Vienna University of Technology, we used the three-hourly pressure level data from the so-called ‘Delayed Cut-off Data Analysis’ (DCDA) stream of the ECMWF over the time period from 2005.0 to 2011.0 with a spatial resolution of 1° . The ‘cut-off time’ is the latest possible arrival time for meteorological observations to

be incorporated in an analysis cycle. Six-hourly and twelve-hourly analysis cycles are combined with short-term forecasts, so that the cut-off time can be delayed and operational products can be made available earlier, as well. A further characteristic is the higher temporal resolution of 3 h that makes use of short-term forecasts.

The use of these data provides some potential for improvements since the known westward propagating waves can be well captured avoiding the need to propagate the $S_2(p)$ standing wave by interpolation. Instead we are able to consider both migrating and non-migrating tidal components. Furthermore, the sampling data permit the proper determination of the $S_1(p)$, $S_2(p)$, and $S_3(p)$ atmospheric tides.

We developed a global gridded model of the $S_1(p)$, $S_2(p)$, and $S_3(p)$ pressure tides using the annual mean model described in Ray and Ponte (2003). Then, sine and cosine amplitudes of each model were convolved with the Green's functions to determine sine and cosine amplitudes of the $S_1(l)$, $S_2(l)$, and $S_3(l)$ tidal loading displacements in vertical and horizontal directions. In the convolution step, we did not invoke the IB assumption but instead considered that the oceanic response at subdaily timescales to the tidal variation in pressure is negligible (Tregoning and Watson 2009).

Since the amplitude of the vertical tidal loading displacement is about three times larger than that in the horizontal displacement, we only show the displacements in the vertical direction in Fig. 7. The displacement magnitude for $S_1(l)$ and $S_2(l)$ reaches 1–2 mm in low latitude regions, but decreases to negligible displacements at the poles. The $S_3(l)$ tidal displacement shows weak latitude dependency and its amplitude is about ten times smaller than those of the $S_1(l)$ and $S_2(l)$ vertical tidal displacements.

It is well known that the $S_1(p)$ atmospheric tide is dominated by large non-migrating components with complicated spatial distributions (Haurwitz and Cowley 1973; Dai and Wang 1999; Ray and Ponte 2003). This signal is susceptible to significant diurnal boundary-layer effects over land masses and land-ocean boundaries. Dai and Wang (1999) mentioned that the upward sensible heat flux from the ground due to solar heating contributes significantly to the non-migrating component of $S_1(p)$. The main migrating component is most apparent over the tropical oceans where the progression of phases shows an approximately constant westward motion. These $S_1(p)$ pressure tide characteristics are well captured in the $S_1(l)$ tidal displacements, where topographic and land-ocean boundary features are clearly seen.

The latent heating associated with convective precipitation, which has a strong diurnal cycle and supplements the direct solar radiational heating, was found to be important mostly for the $S_2(p)$ tide. Therefore, oscillation of the $S_2(p)$ tide is dominated by its migrating component, which is moving westward with the speed of the mean Sun, and is regularly distributed over the globe (Dai and Wang 1999). These $S_2(p)$ pressure tide characteristics can be seen clearly in the $S_2(l)$ tidal displacements.

According to Aso (2003), the ter-diurnal $S_3(p)$ tide has also been detected in the temperature and wind fields in various radar and optical observations. The origin of this tide is still uncertain. If it is a global and migrating tidal wave with zonal wave number three, it is excited either by the third harmonic of heating due to solar insolation absorption by water vapor and ozone or by non-linear interaction of the migrating components of $S_1(p)$ and $S_2(p)$. Interactions between the $S_2(p)$ tide and

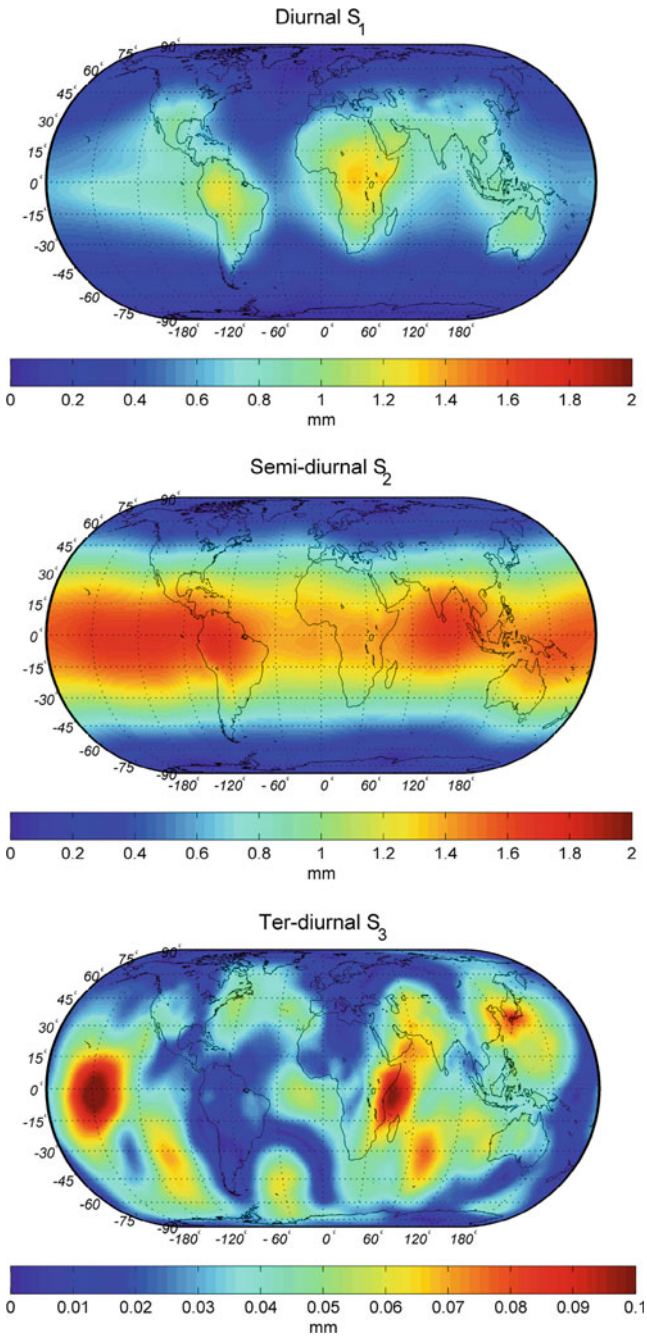


Fig. 7 The amplitude of the $S_1(l)$ (upper panel), $S_2(l)$ (middle panel), and $S_3(l)$ (lower panel) tidal loading displacements in vertical direction

gravity waves can also produce ter-diurnal oscillations. Due to interactions of tidal and gravity waves, the $S_3(p)$ tide is irregularly distributed over the globe (Aso 2003).

2.1.3 APL Services

APL services that provide 6-hourly vertical and horizontal corrections for VLBI, GNSS, SLR sites as well as for the nodes on global grids have been established by several institutions. Each service applies different methods and data to calculate the displacements. Here, we briefly describe three services that provide global models of the displacements from 1980 onward.

- **University of Luxembourg.** The displacements have been derived using the method originally outlined in van Dam and Wahr (1987) with slight modifications in determination of the ocean mask, reference pressure and removing the erroneous atmospheric tides. In van Dam and Wahr (1987), a $2.5^\circ \times 2.5^\circ$ land-sea mask was used. Presently, they use a $0.25^\circ \times 0.25^\circ$ land-sea mask. Units that contain only land are assigned the surface pressure defined by the original NCEP gridded file. Those with only water are assigned the modified IB pressure, defined in van Dam and Wahr (1987). $2.5^\circ \times 2.5^\circ$ grid units containing water and land are subdivided into $0.25^\circ \times 0.25^\circ$ units, each assigned either the land value or the IB value as appropriate. They use a reference pressure determined as a 20 years mean. The pressure data are low pass filtered to remove the erroneous atmospheric tides in the surface pressure data. The filtering means that the online data are always 3–4 days behind the actual date.
- **Goddard Space Flight Center.** The method to calculate the displacements is thoroughly described by Petrov and Boy (2004). Non-tidal loading displacements are determined based on surface pressure data from NCEP with a horizontal resolution of 2.5° . The reference pressure is calculated by averaging 20 years of surface pressure data. To determine tidal loading displacements, the pressure tide model of Ponte and Ray (2002) is used. Petrov and Boy (2004) adopt the method of van Dam and Wahr (1987) to determine the land-sea mask.
- **Vienna University of Technology.** We use surface pressure as derived from pressure level data from operational analysis as well as re-analysis data sets from the ECMWF with a horizontal resolution of 1° . Tidal and non-tidal loading displacements are calculated using the methods described in Sects. 2.1.1 and 2.1.2. The Global Reference Pressure (GRP) model (Schuh et al. 2009) is used to calculate reference pressure. The 6-hourly vertical and horizontal corrections are provided for all VLBI sites as well as for the nodes on a global 1° grid.

Figure 8 shows the displacements at Algonquin Park (ALGOPARK), Canada in vertical and horizontal directions (unit mm) determined by the three APL services. It is obvious that the displacements provided by the Luxembourg and the Petrov and Boy services are very similar with very small differences. The Vienna service produces slightly different results from those of the other two. The difference could

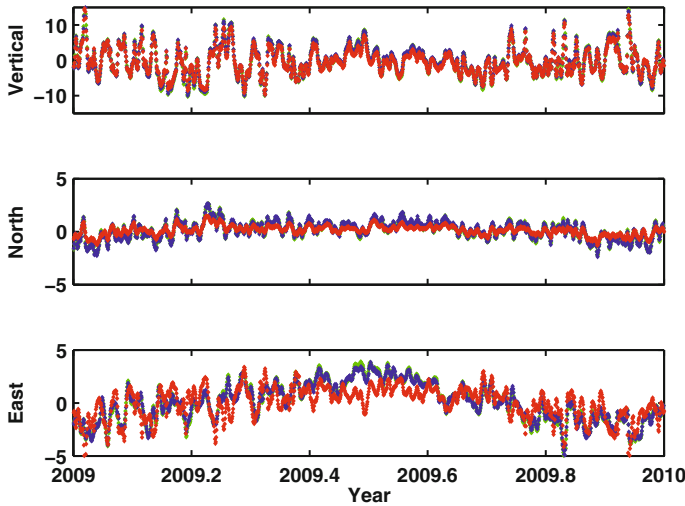


Fig. 8 APL displacements at Algonquin Park (ALGOPARK), Canada in *radial* and *horizontal* directions (unit mm) determined by the three services: Luxembourg (*green*), Petrov and Boy (*blue*) and Vienna (*red*)

be due to different data input (surface versus pressure level, NCEP versus ECMWF) and the land-sea masks used.

2.2 Empirical Model

From Sect. 2.1, it can be seen that APL effects primarily cause vertical displacements of the Earth’s crust and therefore it is possible to determine linear regression coefficients between the size of the vertical displacement and surface pressure variation. To estimate the regression coefficients, Rabbel and Zschau (1985) utilized a geophysical approach (Sect. 2.1) with idealized Gaussian pressure distributions $P(\mathbf{r}) = P_m \exp\left(\frac{-r^2}{r_o^2}\right)$ where P_m is the maximum pressure anomaly at the center of the geometric distribution of cyclones or anticyclones, r is the distance from the center of the distribution, and r_o is the scale length. They found that in general the line of regression between surface pressure and the vertical displacement has the form

$$U_r(\mathbf{r}) = C_1 [P(\mathbf{r}') - P_{ref}(\mathbf{r}')] + C_2 P_m \tag{12}$$

where C_1 and C_2 are the coefficients which are dependent on r_o and $\frac{P(\mathbf{r})}{P_m}$, respectively. They concluded that there is no unique single regression coefficient between local displacements and local surface pressure and that it is therefore also necessary to

Table 1 C_1 coefficients at some space geodetic stations in mm/hPa

Station	GPS	VLBI	Model
	(van Dam et al. 1994)	(MacMillan and Gipson 1994)	(van Dam et al. 1994)
Fairbank	-0.59 ± 0.14	-0.35 ± 0.07	-0.44 ± 0.006
Onsala	-0.00 ± 0.11	-0.16 ± 0.13	-0.29 ± 0.005
Wettzell	-0.30 ± 0.17	-0.53 ± 0.80	-0.43 ± 0.008
Goldstone	-0.80 ± 0.47	-0.30 ± 0.13	-0.40 ± 0.019
Kokee	0.35 ± 0.77	-0.49 ± 0.35	-0.11 ± 0.024

specify the scale length r_o . Their regression coefficient C_1 (mm/hPa) changes from approximately -0.1 mm/hPa at $r_o = 160$ km to -0.9 mm/hPa at $r_o = 5500$ km.

The work of Rabbel and Zschau (1985) had been extended by determining the C_1 coefficient from the vertical displacements as deduced by VLBI (van Dam and Wahr 1987; MacMillan and Gipson 1994; Petrov and Boy 2004) and GNSS (van Dam and Herring 1994; van Dam et al. 1994; Kaniuth and Vetter 2006; Dach et al. 2011) observations. The C_1 coefficient determined by van Dam and Herring (1994) and MacMillan and Gipson (1994) are in the range of -0.4 to -0.6 mm/hPa for inland sites, which corresponds to scale lengths r_o of 1000–2000 km (synoptic scale) in the simple Gaussian pressure model of Rabbel and Zschau (1985). Therefore, most of the variance of APL displacements is determined by synoptic scale pressure variations. This is reasonable since the largest surface pressure variations are synoptic. In most regions of the Earth it should be a good approximation to model the loading effects at a site using only the site pressure.

Table 1 shows the C_1 coefficients at some fundamental stations derived by linear regression between GPS or VLBI vertical positions and local pressure as well as regression between modeled vertical displacement (derived using the method in Sect. 2.1) and local pressure. The coefficients determined by VLBI observations more closely match the coefficients predicted by the model than the GPS results. This may indicate that the loading signal is correlated with another signal in the GPS data processing. GPS or VLBI vertical position estimates and modeled vertical displacements produce different coefficients for Kokee Park, which may be due to inverted barometer effects as this station is located on Kauai, a rather small island in the Pacific Ocean. As Rabbel and Zschau (1985) noted the simple loading functions as given by Eq. (12) can only be applied to anomalous pressure on the continental surface far from any coastlines. On the ocean floor, passing cyclones cause a more complicated effective pressure distribution due to reaction of the water masses. In general, this reaction is dynamical and is affected by water depth, geometry of the coastlines, velocity of the cyclone in a highly complex way. Without any dynamical effects the ocean would react to air pressure changes like an inverse barometer and would compensate an air pressure low by raising the water level so that there is no pressure change on the ocean floor.

3 Study of APL Effects on Space Geodetic Measurements

Studies of APL effects on space geodetic measurements include the detection of the loading signal in the measurements (van Dam and Herring 1994; van Dam et al. 1994; Petrov and Boy 2004), the application of APL corrections at the observation level versus the post-processing level (Tregoning and van Dam 2005; Böhm et al. 2007; Dach et al. 2011), the impact of APL modeling on the precision of the measurements and other parameters (van Dam and Herring 1994; van Dam et al. 1994; Petrov and Boy 2004; Dach et al. 2011). A recent study was carried out by van Dam et al. (2010) who investigated the effects of unmodeled topographic variability on surface pressure estimates and subsequent estimates of vertical surface displacements.

van Dam and Herring (1994) used 1085 VLBI baseline length measurements (1984–1992) from 74 stations to detect the presence of APL signals in the measurements and to investigate the impact of applying APL corrections on the measurement precision. Their analysis indicates that 62 % of APL signal is found in the VLBI baseline residuals. For very accurate measurements, this signal has to be removed in order to avoid misinterpretation of the results. Applying APL effects on the observation level significantly reduces the weighted root-mean-square (WRMS) scatter of the baseline length residuals on 11 of the 22 baselines investigated.

Petrov and Boy (2004) carried out further studies on the presence of APL signals in the VLBI baseline measurements and coordinates. They stated that their approach can estimate the APL displacements with errors less than 15 % of the effect itself. Their analysis of VLBI measurements of 40 stations for the time period from 1980 to 2002 demonstrates that approximately 95 % of the power of modeled vertical pressure loading signal and 97 % of the signal in the baseline lengths is found in VLBI data. They found also that approximately 84 % of the horizontal signal is contained in the VLBI measurements. Neglecting this signal adds noise to the horizontal position with an RMS of 0.6 mm and to the estimates of the EOP with an RMS of $20\mu\text{as}$.

van Dam et al. (1994) assessed the influence of APL effects on GNSS station heights by analyzing daily positions of 20–40 GNSS sites for the time period of approximately 300 days. The application of APL corrections reduces the variance of the station heights by up to 24 % and the WRMS scatter of the baseline length residuals. Approximately 62 % of the investigated GNSS baselines show a reduction in their WRMS scatter. Fifty seven percent of APL signal is evident in the GNSS baseline length measurements. Furthermore, the use of regression coefficients of local pressure measurements appears to be valid at many GNSS sites. However, there are sites where the coefficients are unreliable.

Similar studies were done by Dach et al. (2011) who evaluated the impact of different methods of APL corrections in GNSS data analysis. They applied the corrections from a geophysical model at observation level, on weekly mean estimates of station coordinates at the post processing level, and they also solved for regression coefficients between the station displacements and the local pressure. Analysis of GNSS measurements from IGS stations in the period from 1994 to 2008 showed that the repeatability of station coordinates improves by 20 % when applying the cor-

rections at the observation level and by 10% when applying them as weekly mean values at the post processing level to the resulting weekly coordinates, both compared with a solution without applying APL corrections. Furthermore, Dach et al. (2011) stated that APL corrections via regression coefficients are less beneficial than APL corrections at the observation level. This is due to the fact that the distribution of the pressure in the vicinity of the station has a significant impact on APL displacements and the effects in the horizontal components are completely ignored.

Bock et al. (2005) showed that an improvement of SLR measurements has been obtained when APL effects are modeled, but the magnitude of the improvement is rather small. Furthermore, there appears to be no noticeable effect in the SLR station time bias after accounting for APL effects.

We have studied the performance of the Vienna APL corrections and the Petrov and Boy (2004) models by analyzing 3183 24h VLBI sessions from January 1990 to December 2009. The number of participating stations in each individual session was varying from 3 to 8. Figure 9 shows the difference between the variance of time series of site vertical components with and without applying APL corrections. In general, the application of APL models obviously improves the accuracy of the estimated coordinates, especially for the vertical components and to a lesser degree for the horizontal components (not shown here). We found that the variance of vertical components is deteriorated for only four sites, all of them are located near the coast, after applying either the Vienna-APL model or the Petrov and Boy (2004) model. SC-VLBA and MK-VLBA are placed on Bahamas and Hawaii islands, respectively, while SESHAN25 is near the coast. NL-VLBA is an inland site but it is close to the Great Lakes. Those sites are probably affected by the oceanic response

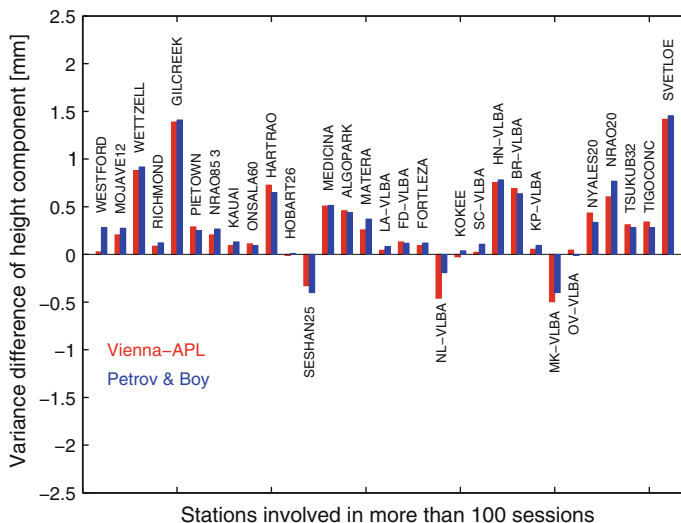


Fig. 9 Variance difference of time series of vertical component. Station name and latitude are plotted above the bar

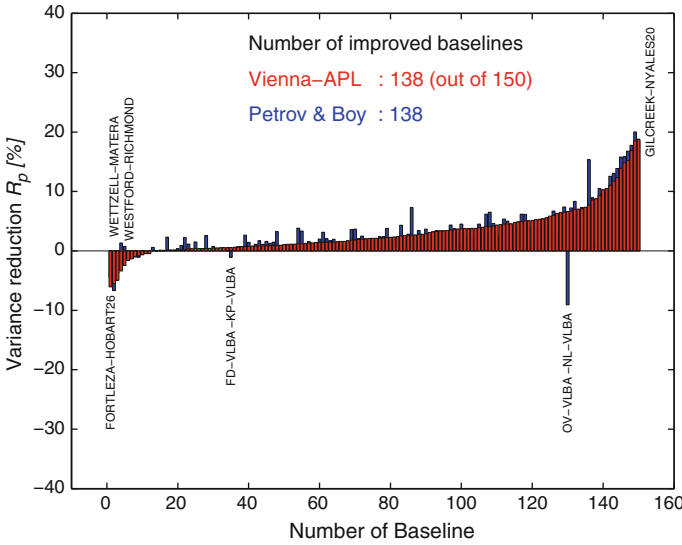


Fig. 10 Variance reduction power R_p of the baseline length residuals after applying the Vienna-APL (red) and the Petrov and Boy (blue) model

that is not adequately modeled in the IB corrections. This holds also for stations on a small island (Kokee Park on Hawaii) and near the coast (RICHMOND, ONSALA60) where the variance of vertical components is either only slightly improved or deteriorated marginally. It can clearly be seen that the biggest improvement is obtained for mid-latitude, inland sites (WETTZEILL, GILCREEK, ALGOPARK, SVETLOE, HARTRAO), which are subject to the largest atmospheric loading effects.

To assess the improvement in power of the baseline repeatability after applying the APL corrections, we analyzed the variance reduction power R_p (in percent) as:

$$R_p = \frac{\Delta\sigma^2}{\sigma_{no-apl}^2} \times 100 \%, \tag{13}$$

where positive R_p will give an indication of baseline improvement when applying an APL model. We plot the variance reduction power R_p in Fig. 10. The use of the Vienna-APL model reduces the variance of the baseline length residuals by as much as 20 % (with the mean variance reduction about 3 %) and improves the repeatability for 85 % (127 out of 150) of the baseline lengths. These improvements are similar those reported by Petrov and Boy (2004) (77 %, 116 out of 150).

Acknowledgments We would like to thank the reviewer, Jean-Paul Boy, for checking this part of the book and providing very valuable suggestions. We are grateful for the financial support from the Austrian Science Fund (FWF, P20902-N10).

References

- T. Aso. An overview of the terdiurnal tide observed by polar radars and optic. *Adv. Polar Upper Atmos. Res.*, 17: 167–176, 2003.
- D. Bock, R. Noomen, and H.G. Scherneck. Atmospheric pressure loading displacement of SLR stations. *J. Geodyn.*, 39: 247–266, 2005.
- J. Böhm, R. Heinkelmann, P.J. Mendes, and H. Schuh. Short note: a global model of pressure and temperature for geodetic applications. *J. of Geod.*, 81 (10):679–683, doi:[10.1007/s00190-007-0135-3](https://doi.org/10.1007/s00190-007-0135-3), 2007.
- J.P. Boy and B.F. Chao. Precise evaluation of atmospheric loading effects on earth's time-variability gravity field. *J. Geophys. Res.*, 110: B08412, doi:[10.1029/2002JB002333](https://doi.org/10.1029/2002JB002333), 2009.
- R. Dach, J. Böhm, S. Lutz, P. Steigenberger, and G. Beutler. Evaluation of the impact of atmospheric pressure loading modeling on GNSS data analysis. *J. Geod.*, 85: 75–91, doi:[10.1007/s00190-010-0417-z](https://doi.org/10.1007/s00190-010-0417-z), 2011.
- A. Dai and J. Wang. Diurnal and semidiurnal tides in global surface pressure fields. *J. of Atm. Science*, 56: 3874–3891, 1999.
- A. Dell'Aquila, V. Lucarni, and P.M. Ruti. Hayashi spectra of the northern hemisphere mid-latitude atmospheric variability in the NCEP-NCAR and ECMWF reanalysis. *Climate Dynamics*, 25: 639–652, 2005.
- W.E. Farrell. Deformation of the earth by surface loads. *Rev. Geophys.*, 10: 751–797, 1972.
- J. Geng, S.D.P. Williams, F.N. Teferle, and A.H. Dodson. Detecting storm surge loading deformations around the southern North Sea using subdaily GPS. *Geophys. J. Int.*, 191: 569–578 doi:[10.1111/j.1365-246X.2012.05656.x](https://doi.org/10.1111/j.1365-246X.2012.05656.x), 2012.
- B. Haurwitz and A.D. Cowley. The diurnal and semidiurnal barometric oscillations, global distribution and annual variation. *Pure Appl. Geophys.*, 102: 193–222, 1973.
- B. Hofmann-Wellenhof and H. Moritz. *Physical Geodesy*. pringer, Wien - New York, 2005.
- K. Kaniuth and S. Vetter. Estimating atmospheric pressure loading regression coefficients from gps observations. *GPS Solut.*, 10: 126–134, doi:[10.1007/s10291-005-0014-4](https://doi.org/10.1007/s10291-005-0014-4), 2006.
- D.S. MacMillan and J.M. Gipson. Atmospheric pressure loading parameters from very long baseline interferometry observations. *J. Geophys. Res.*, 99 (B9): 18,081–18,087, doi:[10.1029/94JB01190](https://doi.org/10.1029/94JB01190), 1994.
- G. Petit and B. Luzum. IERS Conventions 2010. Technical Report 36, IERS Technical Note, 2010.
- L. Petrov and J.P. Boy. Study of the atmospheric pressure loading signal in very long baseline interferometry observations. *J. Geophys. Res.*, 109 (B03405): 1–14, doi:[10.1029/2003JB002500](https://doi.org/10.1029/2003JB002500), 2004.
- R.M. Ponte and R.D. Ray. Atmospheric pressure corrections in geodesy and oceanography: A strategy for handling air tides. *Geophys. Res. Lett.*, 29 (24): 2153–2156, doi:[10.1029/2002GL016340](https://doi.org/10.1029/2002GL016340), 2002.
- W. Rabbel and J. Zschau. Static deformation and gravity changes at the earth's surface due to atmospheric loading. *J. Geophys.*, 56:81–99, 1985.
- R.D. Ray and R.M. Ponte. Barometric tides from ECMWF operational analyses. *Ann. Geophys.*, 21:1897–1910, 2003.
- H. Schuh, M. Schindelegger, D.D. Wijaya, J. Böhm, and D.A. Salstein. Memo: A method for the definition of global reference pressure. http://www.ggosatm.hg.tuwien.ac.at/LOADING/REFPRES/global_reference_pressure_memo.pdf, 2009
- P. Tregoning and T.M. van Dam. Atmospheric pressure loading corrections applied to GPS data at the observation level. *Geophys. Res. Lett.*, 32:L22310, doi:[10.1029/2005GL024104](https://doi.org/10.1029/2005GL024104), 2005.
- P. Tregoning and C. Watson. Atmospheric effects and spurious signals in GPS analysis. *J. Geophys. Res.*, 114 (B09403, 15 PP.): doi:[10.1029/2009JB006344](https://doi.org/10.1029/2009JB006344), 2009.
- T.M. van Dam, G. Blewitt, and M.B. Hefflin. Atmospheric pressure loading effects on global positioning system coordinate determinations. *J. Geophys. Res.*, 99 (B12): 23,939–23,950, doi:[10.1029/94JB02122](https://doi.org/10.1029/94JB02122), 1994.

- T.M. van Dam and J. Wahr. Displacements of the earth's surface due to atmospheric loading: Effects on gravity and baseline measurements. *J. Geophys. Res.*, 92 (B2): 1281–1286, doi:[10.1029/JB092iB02p01281](https://doi.org/10.1029/JB092iB02p01281), 1987.
- T.M. van Dam and T.A. Herring. Detection of atmospheric pressure loading using very long baseline interferometry measurements. *J. Geophys. Res.*, 99 (B3): 4505–4517, doi:[10.1029/93JB02758](https://doi.org/10.1029/93JB02758), 1994.
- T.M. van Dam, Z. Altamimi, X. Collilieux, and J. Ray. Topographically induced height errors in predicted atmospheric loading effects. *J. Geophys. Res.*, 115 (B07415, 10 PP.): doi:[10.1029/2009JB006810](https://doi.org/10.1029/2009JB006810), 2010.
- H. van den Dool, S. Saha, J. Schemm, and J. Huang. A temporal interpolation method to obtain hourly atmospheric surface pressure tides in reanalysis 1979–1995. *J. Geophys. Res.*, 102 (D18): 22,013–22,024, doi:[10.1029/97JD01571](https://doi.org/10.1029/97JD01571), 1997.
- J.M. Wahr. The effects of the atmosphere and oceans on the Earth's wobble and on the seasonal variations in the length of day - II. Results. *Geophysical Journal of the Royal Astronomical Society*, 74: 451–487, 1983.
- J.M. Wallace and P.V. Hobbs. *Atmospheric science: an introductory survey*. Academic Press, 2nd edition, 2006.
- D. Wunsch and D. Stammer. Atmospheric loading and the oceanic “inverted barometer” effects. *Rev. Geophys.*, 35: 79–107, 2010.